

Robust Stochastically-Descending Unrolled Networks

Samar Hadou, Navid NaderiAlizadeh, and Alejandro Ribeiro

Abstract—Deep unrolling, or unfolding, is an emerging learning-to-optimize method that unrolls a truncated iterative algorithm in the layers of a trainable neural network. However, the convergence guarantees and generalizability of the unrolled networks are still open theoretical problems. To tackle these problems, we provide deep unrolled architectures with a stochastic descent nature by imposing descending constraints during training. The descending constraints are forced layer by layer to ensure that each unrolled layer takes, on average, a descent step toward the optimum during training. We theoretically prove that the sequence constructed by the outputs of the unrolled layers is then guaranteed to converge for unseen problems, assuming no distribution shift between training and test problems. We also show that standard unrolling is brittle to perturbations, and our imposed constraints provide the unrolled networks with robustness to additive noise and perturbations. We numerically assess unrolled architectures trained under the proposed constraints in two different applications, including the sparse coding using learnable iterative shrinkage and thresholding algorithm (LISTA) and image inpainting using proximal generative flow (GLOW-Prox), and demonstrate the performance and robustness benefits of the proposed method.

Index Terms—Algorithm Unrolling, Deep Unfolding, Learning to Optimize, Constrained Learning.

I. INTRODUCTION

Learning-based approaches have provided unprecedented performance in many applications in the realm of signal processing. Due to the wide availability of data nowadays and recent advancements in hardware infrastructure, these learning-based approaches often outperform their traditional model-based alternatives, where the models are handcrafted based on domain knowledge. This is particularly true because of the large number of parameters used therein that can approximate complicated mappings otherwise difficult to characterize precisely. Furthermore, the number of layers in deep neural networks is usually much smaller than the number of iterations required in a traditional iterative algorithm, and modern computational platforms are optimized to execute the core operations of these networks efficiently. Therefore, learning-based methods provide a computational advantage over their traditional counterparts during inference.

However, deep networks are purely data-driven, and their structures are, therefore, hard to interpret, which is a serious concern in safety-critical applications, such as medical imaging and autonomous driving. In contrast, model-based methods are highly interpretable since they exploit prior domain knowledge to model the underlying physical process. Moreover, the lack of any prior domain knowledge prevents deep networks from

generalizing well to unseen problems when abundant high-quality data is not available.

To combine the benefits of the two aforementioned regimes, the seminal work of [1] has introduced *algorithm unrolling*, or unfolding. Algorithm unrolling is a *learning-to-optimize* technique that unrolls the iterations of an iterative algorithm through the layers of a customized deep neural network. Under this framework, the unrolled networks can be thought of as an iterative optimizer that is designed based on prior domain knowledge and whose parameters are learnable. Thus these unrolled networks inherit the interpretability of iterative models. Beyond its interpretability, unrolling inversely contributes to the elucidation of deep neural networks by viewing them as the unfolding of an optimization process [2]–[4]. In addition, unrolled networks typically have much fewer parameters compared to traditional deep neural networks, which alleviates the requirement of massive training datasets. An additional advantage of unrolling manifests in accelerated convergence rates, requiring substantially fewer layers (i.e., iterations) while concurrently achieving superior performance compared to standard iterative models [5]. The efficacy of unrolling is evident through its notable success in many applications such as computer vision [6]–[10], wireless networks [11]–[16], medical imaging [17]–[20], and even training neural networks [21], [22], among many others [23]–[26].

Deriving convergence guarantees is an essential theoretical question that arises when developing an iterative algorithm. Since unrolled optimizers resemble algorithms that are widely known to be convergent, this might imply convergence guarantees of the unrolled algorithms by default. However, this is not the case. The more parameters of the iterative algorithm we set free to learn, the wider the subspace of unrolled models we search and the harder it is to find a convergent model. As a toy example, Figure 1 shows trajectories to a stationary point of a convex function made by both gradient descent (GD) and an unrolled version of it, where we make the descent direction learnable. Unlike gradient descent (left), the unrolled network (middle) moves randomly and in opposite directions, before eventually jumping to a near-optimal point in the last one or two layers. This is not surprising since the training procedure of the unrolled network does not regulate the trajectories across the intermediate unrolled layers.

The lack of convergence across the unrolled layers engenders two critical issues despite the superior performance achieved at the last layers. First, the lack of convergence guarantees limits our ability to draw conclusions about the generalizability of these models to unseen problems. Contrarily, standard iterative algorithms are endowed with theoretical convergence guarantees, thereby eliminating any doubts about their generalizability. Second, unrolled networks are brittle to perturbations added to the layers’ outputs due to the lack of convergence guarantees.

S. Hadou and A. Ribeiro are with the Department of Electrical and Systems Engineering, University of Pennsylvania. Emails: {selaraby, aribeiro}@seas.upenn.edu. N. NaderiAlizadeh is with the Department of Biostatistics and Bioinformatics, Duke University. Email: navid.naderi@duke.edu

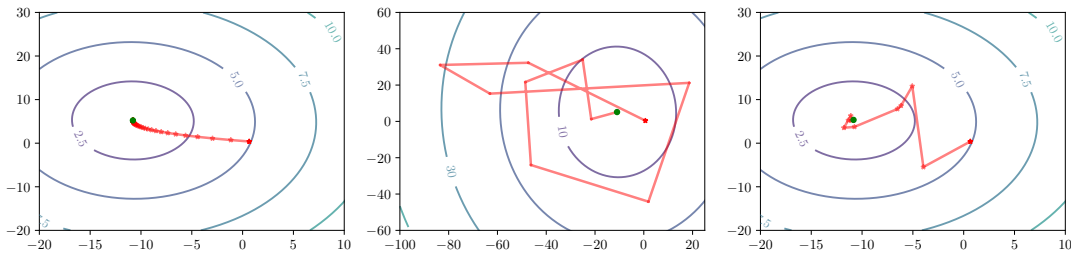


Fig. 1: Trajectories of a test example made by (left) gradient descent, (middle) a standard unrolled optimizer, and (right) a constrained unrolled optimizer (ours). The three trajectories were initialized with the same value. The colored contours represent the values of the objective function that is being minimized (least squares).

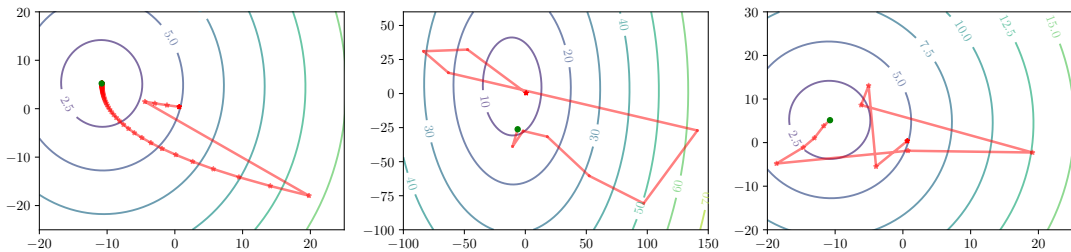


Fig. 2: Trajectories of the same test example initialized at the same point but perturbed at the third step with additive noise. The center of the colored contours represents the optimal point, and the final estimate of the optimizers is depicted in green. The standard unrolled optimizer (middle) fails to reach the optimum under additive perturbations, while the constrained one (right), as well as gradient descent (left), succeeds in doing so.

In contrast, standard iterative algorithms with descending guarantees, like GD, are known to be resilient to perturbations as they would still follow a descending direction in the iterations that follow the one where the perturbation occurs (see Figure 2 (left)). This evidently does not extend to their unrolled counterparts since they lack descending guarantees. Revisiting our example, Figure 2 (middle) confirms this fact as the unrolled optimizer fails to converge to the same point as in Figure 1 (middle) after adding perturbations to one of its layers; in fact, the figure shows that the distance to the optimal at the last layer is larger than it is at initialization. This raises concerns about implementing these models in safety-critical applications.

Previous works have investigated the convergence issue of algorithm unrolling. One approach for providing convergence guarantees, known as safeguarding, has been proposed in [27]–[30]. The main idea of safeguarding is to check whether the estimate made by a certain layer, during inference, satisfies some form of descent criteria. If the criteria are not satisfied, the estimate is discarded and replaced with an estimate of the classic iterative algorithm. Another line of work proved the existence of a convergent unrolled network for specific iterative algorithms such as the iterative shrinkage and thresholding algorithm (ISTA) [31], [32] and differentiable linearized ADMM [33]. However, a mechanism that guarantees to find these convergent networks was never provided. To resolve this issue, [32], [34] suggest reducing the size of the search space by learning fewer parameters of the standard algorithm, which limits the network’s expressivity. Furthermore, all these

theoretical endeavors are tailored for specific optimization algorithms and do not generalize to other algorithms. This leaves many existing and potential unrolled networks without convergence guarantees.

In this paper, we aim to design unrolled algorithms that are stochastically descending as in Figure 1 (right) and robust to additive perturbations as in Figure 2 (right). On top of that, our goal is to provide theoretical convergence guarantees for unrolled networks regardless of the underlying iterative algorithms. We accomplish this by posing the training problem as a *constrained learning* problem. Under this constrained formulation of the problem, we force each unrolled layer to take a descent direction, on average. This descent direction need not be the gradient direction, as shown in Figure 1 (right), in order to accelerate convergence even for harder landscapes. To complement our endeavor, we theoretically derive convergence guarantees for unrolled networks trained with our descending constraints and prove exponential rates of convergence. In summary, our contributions are as follows:

- We develop the use of descending constraints in training unrolled optimizers to provide them with descending properties (Sections III-A and III-B).
- We rigorously prove that an unrolled network trained under our framework is guaranteed to converge to a near-optimal region infinitely often (Section III-C).
- We empirically show the robustness of these unrolled networks to perturbations in light of two applications: sparse coding (Section IV) and image inpainting (Section V).

II. PROBLEM FORMULATION

Consider a differentiable function f drawn from the function class $\mathfrak{F} = \{f(\cdot; \mathbf{x}) | \mathbf{x} \in \mathcal{X}\}$, where \mathcal{X} is a compact set. The ultimate goal of algorithm unrolling is to learn an L -layered neural optimizer Φ that converges to a stationary point of the function $f(\cdot; \mathbf{x})$ for any \mathbf{x} . This optimizer Φ is parameterized by a sequence of parameters $\mathbf{W} = \{\mathbf{W}_l\}_{l=1}^L$, each of which resembles the parameters of an iterative optimization algorithm, e.g., proximal gradient descent. The outputs of the unrolled layers form an L -long trajectory of estimates, with the ideal goal of descending towards a stationary point.

Learning the optimizer Φ can then be expressed as the bi-level optimization problem,

$$\begin{aligned} \min_{\mathbf{W}} \quad & \mathbb{E}[\ell(\Phi(\mathbf{x}; \mathbf{W}), \mathbf{y}^*)] && \text{(Optimizer)} \\ \text{s.t.} \quad & \mathbf{y}^* \in \underset{\mathbf{y} \in \mathcal{Y}}{\text{argmin}} f(\mathbf{y}; \mathbf{x}), \quad \forall \mathbf{x} \in \mathcal{X}. && \text{(Optimizee)} \end{aligned}$$

The inner problem is an instantiation of finding a minimum of $f(\cdot; \mathbf{x})$ for a given \mathbf{x} , which we refer to as the optimizee. It, however, needs to be evaluated for all $\mathbf{x} \in \mathcal{X}$, which is computationally expensive. The outer problem aims to learn the optimizer $\Phi: \mathcal{X} \rightarrow \mathcal{Y}$ by minimizing a suitably-chosen loss function $\ell: \mathcal{Y} \times \mathcal{Y} \rightarrow \mathbb{R}$. For instance, the toy example in Figure 1 considers a function class \mathfrak{F} that contains functions of the form $f(\mathbf{y}; \mathbf{A}, \mathbf{z}) = \|\mathbf{A}\mathbf{y} - \mathbf{z}\|_2$, which is parameterized by $\mathbf{A} \in \mathcal{S}$ and $\mathbf{z} \in \mathcal{Z}$ with $\mathcal{X} \equiv \mathcal{S} \times \mathcal{Z}$. The optimizee problem is then to find the stationary point of f for each combination of \mathbf{A} and \mathbf{z} in \mathcal{X} . The optimizer Φ , in this case, is designed by unrolling GD in L layers, each of which is a multilayer perceptron (MLP) with residual connections, i.e., the l th layer's output is $\mathbf{y}_l = \mathbf{y}_{l-1} - \text{MLP}(\mathbf{y}_{l-1}, \mathbf{A}, \mathbf{z}; \mathbf{W}_l)$. These MLPs are trained by minimizing the mean-square error (MSE) between the final prediction of Φ and the optimal \mathbf{y}^* .

Solving the above bi-level optimization problem is not usually straightforward. However, it reduces to an unconstrained problem if the inner problem either has a closed-form solution or can be solved using an iterative algorithm. For our problems of interest, we assume that there exists an iterative algorithm \mathcal{A} that finds a (local) minimum \mathbf{y}^* of the optimizee problem. Given algorithm \mathcal{A} and, therefore, the optimal solution to the optimizee, the optimizer problem can be then simplified to

$$\underset{\mathbf{W}}{\text{argmin}} \quad \mathbb{E}[\ell(\Phi(\mathbf{x}; \mathbf{W}), \mathbf{y}^*)]. \quad (1)$$

This form resembles the empirical risk minimization (ERM) problem used in supervised learning, where a model Φ learns to map a given input \mathbf{x} to its label \mathbf{y}^* with little to no restrictions on the intermediate layers of Φ .

It is pertinent to recall that the model Φ in (1) is designed to mimic an iterative descending algorithm, where the output of each layer needs to take a step closer to the optimum. This behavior is not mandated by the loss function in (1) since there is no *regularization* on the outputs of the optimizer's intermediate layers. The absence of regularization leads to the behavior in Figure 1 (middle), where the unrolled optimizer hits the optimum at the last layer while the trajectory to the optimum is not what we expect from a standard descending algorithm.

Since standard unrolling does not necessarily generate descending trajectories, they lack the convergence guarantees, inherent in standard optimization algorithms. This raises concerns about the generalizability of the unrolled optimizer, trained over finite samples from the data distribution, to unseen in-distribution functions $f(\cdot; \mathbf{x}) \in \mathfrak{F}$.

Yet another issue regarding the stability of unrolled optimizers becomes apparent when encountering additive perturbations [35]–[37]. Due to convergence guarantees, standard algorithms are guaranteed to continue descending even after perturbing their trajectories with additive noise. Reverting to our example, Figure 2 (middle) is evidence that this feature is not guaranteed for standard unrolled networks, which raises concerns about their stability.

To put it briefly, lacking convergence guarantees prompts concerns pertaining to generalizability and vulnerability to perturbations. In the following section, we tackle this issue by *imposing descending constraints* over the intermediate layers. Under these constraints, we can think of the unrolled optimizers as stochastic descent algorithms, for which we can provide convergence guarantees.

Remark II.1. While we only train unrolled optimizers in a supervised manner in this paper (c.f. (1)), our problem formulation and proposed method extend to the unsupervised case, where the optimal \mathbf{y}^* is expensive to obtain. The learning problem then can be seen as directly minimizing f , i.e.,

$$\underset{\mathbf{W}}{\text{argmin}} \quad \mathbb{E}[f(\Phi(\mathbf{x}; \mathbf{W}))]. \quad (2)$$

This approach is commonly used in the *learning-to-learn* literature, e.g., [21], [22], [38], [39].

III. CONSTRAINED UNROLLED OPTIMIZERS

To provide unrolled algorithms with convergence guarantees, we propose the use of descending constraints in training the unrolled optimizers relying on constrained learning theory (CLT) [40]. The posed constrained learning problem (CO), while it may initially appear complex, is akin to a regularized ERM problem where the regularization parameter is a (dual) optimization variable to be learned. The key advantage of our approach over a typical regularized problem stems from the sensitivity interpretation of the dual variables [41], which easily discerns constraints that are harder to satisfy. This, in turn, grants us informed insights on which constraints to relax, if possible, during the design phase. In this section, we delineate our method to design these constrained unrolled optimizers by providing a detailed explanation of i) our choice of the descending constraints to employ, ii) the algorithm that solves the constrained problem and provides a probably near-optimal near-feasible solution, and iii) the convergence guarantees bestowed upon these optimizers.

A. Descending Constraints

To force the unrolled optimizer Φ to produce descending trajectories across its layers, we consider two different forms of descending constraints. The first ensures that the gradient

norm of the objective function f decreases over the layers on average, i.e., for each layer $l = 1, \dots, L$, we have

$$\mathbb{E}[\|\nabla f(\mathbf{y}_l; \mathbf{x})\|_2 - (1 - \epsilon) \|\nabla f(\mathbf{y}_{l-1}; \mathbf{x})\|_2] \leq 0, \quad (\text{CI})$$

where \mathbf{y}_l is the l -th unrolled layer's output, $\mathbf{y}_L = \Phi(\mathbf{x}; \mathbf{W})$ is the final estimate, and $\epsilon \in (0, 1)$ is a design parameter. The second forces the distance to the optimal to shrink over the layers, that is,

$$\mathbb{E}[\|\mathbf{y}_l - \mathbf{y}^*\|_2 - (1 - \epsilon) \|\mathbf{y}_{l-1} - \mathbf{y}^*\|_2] \leq 0. \quad (\text{CII})$$

The initial value \mathbf{y}_0 is drawn from a Gaussian distribution $\mathcal{N}(\mu_0, \sigma_0^2 \mathbf{I})$. We also add noise vector \mathbf{n}_l , sampled from a Gaussian distribution $\mathcal{N}(0, \sigma_l^2 \mathbf{I})$, to the output \mathbf{y}_l before it is fed to the next layer to make the constraints statistically independent. The noise variance σ_l^2 decreases over the layers to allow the optimizer to converge.

Having these two constraints in place, we re-write (1) as the following constrained learning problem

$$\begin{aligned} P^* &= \min_{\mathbf{W}} \mathbb{E}[\ell(\Phi(\mathbf{x}; \mathbf{W}), \mathbf{y}^*)] \\ \text{s.t.} \quad &\mathbb{E}[\mathcal{C}(\mathbf{y}_l, \mathbf{y}_{l-1})] \leq 0, \quad \forall l \leq L, \\ &\mathbf{y}_l = \phi(\mathbf{y}_{l-1}; \mathbf{W}_l) + \mathbf{n}_l, \quad 0 < l \leq L, \end{aligned} \quad (\text{CO})$$

where $\mathcal{C}(\cdot, \cdot)$ refers to the loss function in either (CI) or (CII), and $\phi(\cdot; \mathbf{W}_l)$ represents a layer in Φ parameterized by \mathbf{W}_l . The second set of constraints in (CO) should be perceived as implicit constraints that are imposed by default in the structure of the unrolled optimizer Φ and, therefore, omitted in the following analysis.

It is worth noting that the choice between (CI) or (CII) is arbitrary. The former requires the objective function f to be differentiable while the latter depends on the knowledge of the optimal \mathbf{y}^* . Yet (CI) can be extended to non-differentiable functions by replacing the gradient with a subgradient of f . However, (CI) could be more challenging to satisfy if the optimizee problem is either constrained or non-convex. This is true since it could push the estimates to a non-feasible solution in the first instance or another local minimum than \mathbf{y}^* in the second one.

B. Probably and Approximately Correct Solution

To solve (CO), we construct the dual problem to leverage CLT [40, Theorem 1]. The dual problem of (CO) is equivalent to finding the saddle point of the Lagrangian function

$$\mathcal{L}(\mathbf{W}, \boldsymbol{\lambda}) = \mathbb{E}[\ell(\Phi(\mathbf{x}; \mathbf{W}), \mathbf{y}^*)] + \sum_{l=1}^L \lambda_l \mathbb{E}[\mathcal{C}(\mathbf{y}_l, \mathbf{y}_{l-1})], \quad (3)$$

where $\boldsymbol{\lambda} \in \mathbb{R}_+^L$ is a vector collecting the dual variables λ_l . Since evaluating the expectation over an unknown distribution is not attainable, we resort to using an *empirical* Lagrangian function

$$\widehat{\mathcal{L}}(\mathbf{W}, \boldsymbol{\lambda}) = \widehat{\mathbb{E}}[\ell(\Phi(\mathbf{x}; \mathbf{W}), \mathbf{y}^*)] + \sum_{l=1}^L \lambda_l \widehat{\mathbb{E}}[\mathcal{C}(\mathbf{y}_l, \mathbf{y}_{l-1})], \quad (4)$$

Algorithm 1 Primal-Dual Training Algorithm for (CO)

- 1: **Input:** Dataset $\{(\mathbf{x}_n, \mathbf{y}_n^*) \sim \mathcal{D}\}_{n=1}^N$.
- 2: Initialize $\mathbf{W} = \{\mathbf{W}_l\}_{l=1}^L$ and $\boldsymbol{\lambda} = \{\lambda_l\}_{l=1}^L$.
- 3: **for** each epoch **do**
- 4: **for** each batch **do**
- 5: Compute $\widehat{\mathcal{L}}(\mathbf{W}, \boldsymbol{\lambda})$ as in (4).
- 6: Update the primal variable:

$$\mathbf{W} \leftarrow [\mathbf{W} - \mu_w \nabla_{\mathbf{W}} \widehat{\mathcal{L}}(\mathbf{W}, \boldsymbol{\lambda})]. \quad (5)$$

- 7: Update the dual variable:

$$\boldsymbol{\lambda} \leftarrow [\boldsymbol{\lambda} + \mu_\lambda \nabla_{\boldsymbol{\lambda}} \widehat{\mathcal{L}}(\mathbf{W}, \boldsymbol{\lambda})]_+. \quad (6)$$

- 8: **Return:** $\mathbf{W}^* \leftarrow \mathbf{W}$.
-

where $\widehat{\mathbb{E}}$ denotes the sample mean evaluated over N realizations $\{(\mathbf{x}_n, \mathbf{y}_n^*)\}_{n=1}^N$. We then define the empirical dual problem as

$$\widehat{D}^* = \max_{\boldsymbol{\lambda} \in \mathbb{R}_+^L} \min_{\mathbf{W}} \widehat{\mathcal{L}}(\mathbf{W}, \boldsymbol{\lambda}). \quad (\text{DO})$$

Solving (DO) and finding the saddle point of $\widehat{\mathcal{L}}$ is doable by alternating between minimizing with respect to \mathbf{W} for a fixed $\boldsymbol{\lambda}$ and then maximizing the latter, as described in Algorithm 1. The convergence of this algorithm has been proved in [40, Theorem 2].

Nevertheless, Algorithm 1 only finds a solution to (DO), which is not equivalent to the primal problem (CO) that we aim to solve. The difference between the two problems is due to an *approximation* gap and *estimation* gap induced by replacing the statistical expectations with empirical ones. A characterization of this gap is provided by CLT under the following assumptions:

Assumption 1. The functions $\ell(\cdot, \mathbf{y})$ and $\mathcal{C}(\cdot, \mathbf{y})$ are M -Lipschitz continuous for all \mathbf{y} and bounded. The objective function $f(\cdot; \mathbf{x})$ is also M -Lipschitz continuous for all \mathbf{x} .

Assumption 2. Let $\phi_l \circ \dots \circ \phi_1 \in \mathcal{P}_l$ be a composition of l unrolled layers, each of which is parameterized by $\mathbf{W}_i, i \leq l$, and $\overline{\mathcal{P}}_l = \overline{\text{conv}}(\mathcal{P}_l)$ be the convex hull of \mathcal{P}_l . Then, for each $\overline{\phi}_l \circ \dots \circ \overline{\phi}_1 \in \overline{\mathcal{P}}$ and $\nu > 0$, there exists $\mathbf{W}_{1:l}$ such that $\mathbb{E}[\|\phi_l \circ \dots \circ \phi_1(\mathbf{x}; \mathbf{W}_{1:l}) - \overline{\phi}_l \circ \dots \circ \overline{\phi}_1(\mathbf{x})\|] \leq \nu$.

Assumption 3. The set \mathcal{Y} is compact, the conditional distribution $p(\mathbf{x}|\mathbf{y}^*)$ is non-atomic for all \mathbf{y}^* , and the functions $\mathbf{y} \rightarrow \ell(\Phi(\cdot, \mathbf{y}))p(\cdot|\mathbf{y})$ and $\mathbf{y} \rightarrow \mathcal{C}(\Phi(\cdot, \mathbf{y}))p(\cdot|\mathbf{y})$ are uniform continuous in the total variation topology for all $\Phi \in \overline{\mathcal{P}}_l, l \leq L$.

Assumptions 2 and 3 aim to establish a connection between (CO) and its functional counterpart that learns a composition of L functions $\overline{\phi}_L \circ \dots \circ \overline{\phi}_1 \in \overline{\mathcal{P}}_L$. Assumption 3 asserts a zero duality gap between the functional problem and its dual while Assumption 2 ensures that the parameterization \mathbf{W} is rich enough to approximate the functional space $\overline{\mathcal{P}}_L$. Through these assumptions, CLT analyzes the change to the duality gap of the functional problem when it is approximated by (CO). On the other hand, CLT characterizes the estimation gap through the sample complexity indicated by Assumption 4. Moreover,

CLT requires the problem to be strictly feasible, as described in Assumption 5.

Assumption 4. There exists $\zeta(N, \delta) \geq 0$ that is monotonically decreasing with N , for which it holds with probability $1 - \delta$ that $|\mathbb{E}[\ell(\Phi(\mathbf{x}; \mathbf{W}), \mathbf{y}^*)] - \widehat{\mathbb{E}}[\ell(\Phi(\mathbf{x}; \mathbf{W}), \mathbf{y}^*)]| \leq \zeta(N, \delta)$ and $|\mathbb{E}[\mathcal{C}(\mathbf{y}_l, \mathbf{y}_{l-1})] - \widehat{\mathbb{E}}[\mathcal{C}(\mathbf{y}_l, \mathbf{y}_{l-1})]| \leq \zeta(N, \delta)$ for all l .

Assumption 5. There exists $\Phi \in \mathcal{P}_L$ that is strictly feasible, i.e., $\mathbb{E}[\mathcal{C}(\mathbf{y}_l, \mathbf{y}_{l-1})] \leq -M\nu - \xi$ and $\widehat{\mathbb{E}}[\mathcal{C}(\mathbf{y}_l, \mathbf{y}_{l-1})] \leq -\xi$ for all $l \leq L$, with M and ν as in Assumptions 1 and 2 and $\xi > 0$.

CLT then asserts that a stationary point of (DO) provides a probably, approximately correct solution to (CO).

Theorem 1 (CLT [40]). *Let $(\mathbf{W}^*, \lambda^*)$ be a stationary point of (DO). Under Assumptions 1- 5, it holds, for some constant ρ , that*

$$|P^* - \widehat{D}^*| \leq M\nu + \rho \zeta(N, \delta), \text{ and} \quad (7)$$

$$\mathbb{E}[\mathcal{C}(\mathbf{y}_l, \mathbf{y}_{l-1})] \leq \zeta(N, \delta), \quad \forall l, \quad (8)$$

with probability $1 - \delta$ each and with $\rho \geq \max\{\|\lambda^*\|, \|\bar{\lambda}^*\|\}$, where $\bar{\lambda}^* = \arg\max_{\lambda} \min_{\mathbf{W}} \mathcal{L}(\mathbf{W}, \lambda)$.

As per Theorem 1, the solution \mathbf{W}^* is near-optimal and near-feasible. Moreover, the duality gap depends on a smoothness constant M , the richness parameter ν , the sample complexity $\zeta(N, \delta)$, and the sensitivity to the constraints embodied by the dual variables λ^* .

Theorem 1 also implies that an optimizer trained via Algorithm 1 satisfies the descending constraints at each layer up to a fixed margin with a probability of $1 - \delta$. This margin solely depends on the sample complexity, which can be kept small by increasing the number of samples N . This result postulates that at each layer, the unrolled optimizer with a high probability takes a step closer to an optimal point of the optimizee. As a consequence, the trained optimizer can be interpreted as a *stochastic* descent algorithm.

C. Convergence Guarantees

The above result does not directly guarantee that the sequence $\{\mathbf{y}_l\}_{l=1}^L$ obtained at the outputs of the unrolled layers *converges* to a stationary point of the function $f(\mathbf{y}; \cdot)$. The probably, approximately correct solution we have attained only satisfies the descending constraints with a probability $1 - \delta$. Even for small values of δ , the probability that all the constraints are satisfied together, which is $(1 - \delta)^L$, is exponentially decreasing with the number of layers L . Therefore, a rigorous analysis is still required to affirm the convergence guarantees of unrolled optimizers. In Theorem 2, we confirm that the unrolled optimizer trained under constraints (CI) indeed has convergence guarantees.

Theorem 2. *Given are a near-optimal solution of (CO) under constraints (CI), which satisfies (8) with a probability $1 - \delta$ and generates a sequence of random variables $\{\mathbf{y}_l\}_{l=1}^L$. Then, under Assumption 1, it holds that*

$$\lim_{l \rightarrow \infty} \mathbb{E} \left[\min_{k \leq l} \|\nabla f(\mathbf{y}_k; \mathbf{x})\| \right] \leq \frac{1}{\epsilon} \left(\zeta(N, \delta) + \frac{\delta M}{1 - \delta} \right) \text{ a.s.} \quad (9)$$

with $\zeta(N, \delta)$ as described in Assumption 4.

Proof. The proof is relegated to Appendix A. \square

Theorem 2 states that the sequence $\{\mathbf{y}_l\}_l$ infinitely often visits a region around the optimal where the expected value of the gradient norm hits a value under $\frac{1}{\epsilon}(\zeta(N, \delta) + \frac{\delta M}{1 - \delta})$. This near-optimal region is determined by the sample complexity of Φ , the Lipschitz constant M , and a design parameter ϵ of the constraints. The same analysis can be conducted for the case when the constraints (CII) is considered leading to similar guarantees.

The convergence rate of the unrolled network trained according to (CO) is derived in Lemma 1. As per this lemma, the expected value of the gradient norm drops exponentially with the number of unrolled layers L . This result is explicable through the recursive nature of the imposed constraints.

Lemma 1. *For a trained unrolled optimizer \mathbf{W}^* that satisfies Theorem 1, the gradient norm achieved after L layers satisfies*

$$\mathbb{E}[\|\nabla f(\mathbf{W}_L)\|] \leq (1 - \delta)^L (1 - \epsilon)^L \mathbb{E}[\|\nabla f(\mathbf{W}_0)\|] + \frac{1}{\epsilon} \left(\zeta(Q, \delta) + \frac{\delta M}{1 - \delta} \right). \quad (10)$$

Proof. The proof can be found in Appendix B. \square

In the following two sections, we consider two use cases, namely sparse coding and inverse problems, where algorithm unrolling achieves superior performance. We aim to show the impact of our proposed descending constraints on the performance and robustness of these two use cases.

IV. CASE STUDY I: LISTA FOR SPARSE CODING

In our first case study, we tackle the sparse coding problem, which is of enduring interest in signal processing. In this section, we provide a brief description of the problem and its iterative solution. We also show the mechanism that has been previously proposed to unroll this iterative algorithm and then provide discussions, supported by numerical simulations, to evaluate the proposed descending constraints.

A. Problem Formulation

Sparse coding refers to the problem of finding a sparse representation of an input signal $\mathbf{x} \in \mathbb{R}^p$ using an overcomplete dictionary $\mathbf{D} \in \mathbb{R}^{p \times d}$ with $d > p$. The goal is to find a sparse code $\mathbf{y} \in \mathbb{R}^d$ that satisfies $\mathbf{x} \approx \mathbf{D}\mathbf{y}$. This optimizee problem can be cast as a LASSO regression problem

$$\min_{\mathbf{y}} \frac{1}{2} \|\mathbf{x} - \mathbf{D}\mathbf{y}\|_2^2 + \alpha \|\mathbf{y}\|_1, \quad (11)$$

where $\alpha > 0$ is a regularization parameter. The ℓ_1 -norm is used as a regularization term to control the sparsity of the solution.

A widely-used method for solving (11) is the iterative shrinkage and thresholding algorithm (ISTA) [42], [43]. At each iteration k , ISTA updates the k -th iteration of the solution, denoted by \mathbf{y}_k , according to the following rule:

$$\mathbf{y}_k = \mathcal{S}_{\alpha/\nu} \left(\mathbf{y}_{k-1} - \frac{1}{\nu} \mathbf{D}^\top (\mathbf{D}\mathbf{y}_{k-1} - \mathbf{x}) \right), \quad (12)$$

where ν is a parameter whose value is larger than the largest eigenvalue of $\mathbf{D}^\top \mathbf{D}$, and $\mathcal{S}_{\alpha/\nu}$ is the soft-thresholding operator,

$$\mathcal{S}_{\alpha/\nu}(\mathbf{y}) = \text{sign}(\mathbf{y}) \cdot \max\{|\mathbf{y}| - \alpha/\nu, 0\}, \quad (13)$$

which is evaluated elementwise. The update rule in (12) performs a proximal gradient descent step, which is equivalent to a gradient step in the direction of $-\nabla \|\mathbf{x} - \mathbf{D}\mathbf{y}\|_2^2/2$ followed by a projection onto the ℓ_1 -norm ball. This projection ensures that the new value \mathbf{y}_k is within the feasible set of the optimizee problem.

B. LISTA: Unrolled Solution

The seminal work in [1] has unrolled the update rule of ISTA and introduced Learnable ISTA (LISTA) for sparse coding contexts. This work has re-identified the iteration in (12) as a linear mapping of \mathbf{y} followed by a nonlinear activation function (i.e., a soft-thresholding function), i.e.,

$$\mathbf{y}_l = \mathcal{S}_{\beta^l}(\mathbf{D}_u^l \mathbf{x} + \mathbf{D}_e^l \mathbf{y}_{l-1}), \quad (14)$$

with $\mathbf{D}_u^l \in \mathbb{R}^{d \times p}$, $\mathbf{D}_e^l \in \mathbb{R}^{d \times d}$ and $\beta^l \in \mathbb{R}^d$ being learnable parameters. Cascading L of these layers in an unrolled architecture is then equivalent to executing ISTA for L iterations. This unrolled architecture has two notable features. First, \mathbf{D}_u^l represents a residual (i.e., skip) connection from the input \mathbf{x} to layer l , which is reminiscent of ResNets. Second, the network employs a parametric nonlinear activation function, which has been a recent trend in designing neural networks [44]–[46].

As can be observed by comparing (14) to (12), LISTA has decoupled its parameters by making the following substitutions: $\mathbf{D}_u = (1/L)\mathbf{D}^\top$ and $\mathbf{D}_e = \mathbf{I} - (1/L)\mathbf{D}^\top \mathbf{D}$. However, the decoupling of \mathbf{D}_u and \mathbf{D}_e was proven to have a negative impact on the convergence of LISTA [31].

C. Constrained LISTA

In our approach, we adopt the same structure of LISTA in (14), but we perform a constrained learning-based training procedure according to (CO). As in [1], the unrolled network is trained by minimizing the mean square error (MSE);

$$\min_{\mathbf{W}} \mathbb{E}[\|\Phi(\mathbf{x}; \mathbf{W}) - \mathbf{y}^*\|_2^2]. \quad \text{s.t. (CII)}. \quad (15)$$

Relying on the constraints (CII) is a deliberate choice that fits the nature of the optimizee problem (11). The optimizee is originally a constrained problem, where the goal is to find a point within the ℓ_1 -norm ball that minimizes the objective function. Following the gradients of the ℓ_2 -norm would not guarantee convergence to a feasible solution unless we add explicit ℓ_1 -norm constraints on the outputs of the unrolled layers.

D. Numerical Results and Discussions

In our experiments, we evaluate the performance of the proposed constrained-learning approach on grayscale CIFAR10 dataset. Each image has 32×32 pixels and is flattened into a 1024-dimensional vector. To fully identify the optimizee problem, using $d = 1228$, we construct the dictionary \mathbf{D} as a random matrix with each element independently drawn from

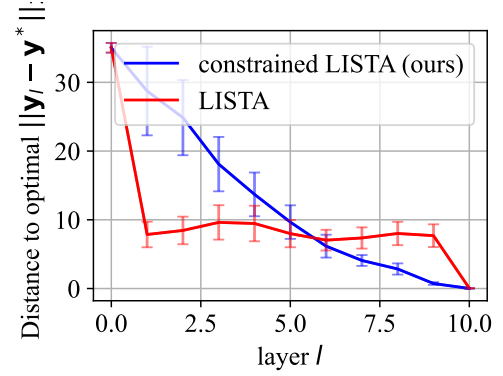


Fig. 3: Distance to the optimal solution \mathbf{y}^* of the sparse coding problem (11) across the unrolled layers of LISTA (red) vs constrained LISTA (blue). The distance does not change significantly at the intermediate layers of LISTA, while constrained LISTA makes gradual progressions toward the optimum.

a Gaussian distribution $\mathcal{N}(0, 1)$ and we set $\alpha = 0.5$. Under this set-up, we evaluate the sparse vector $\mathbf{y}^* \in \mathbb{R}^{1228}$ for each image $\mathbf{x} \in \mathbb{R}^{1024}$ by executing ISTA for 10 thousands iterations and construct a dataset $\{(\mathbf{x}_i, \mathbf{y}_i^*)\}$ to train the unrolled LISTA. The dataset consists of 32×10^3 training, 8×10^3 validation and 10^4 test examples.

The unrolled LISTA consists of $L = 10$ layers. We take the initial estimate \mathbf{y}_0 to be a random vector drawn from $\mathcal{N}(0, \mathbf{I})$, which is then fed to the unrolled network along with the input images. During training, the layers' outputs are contaminated with additive Gaussian noise with zero mean and a variance of $\sigma_l^2 = \hat{\sigma}^2 g_l^2$, where g_l is the gradient at layer l and $\hat{\sigma} = 1$. We train the unrolled model for 30 epochs using ADAM with a learning rate $\mu_w = 10^{-5}$ and a dual learning rate $\mu_\lambda = 10^{-3}$. We also set the constraint parameter ϵ to 0.05.¹

Performance. Figure 3 compares the performance of LISTA and constrained LISTA on a test dataset. The two models achieve the same performance at their outputs, illustrated by the zero distance achieved at the last layer in both cases. However, their behaviors over the intermediate layers differ significantly from each other. For standard LISTA, the distance to the optimal is almost the same across all these layers, which suggests that there was no significant improvement in the estimates. In contrast, constrained LISTA demonstrates a gradual decrease in the distance to the optimum because of the imposed constraints.

To elaborate more on this difference, we show the histogram of the ℓ_1 -norm of the estimates in Figure 4. As shown in the figure, the ℓ_1 -norm of the estimates barely changes between the first and ninth LISTA's layers (shown in red). This suggests that LISTA overlooks the sparsity requirement of the solution altogether, which is aligned with the fact that this requirement is not represented in the MSE training loss that is used in LISTA. Meanwhile, constrained LISTA uses the constraints (CII) to provoke this requirement through all the layers. Therefore, we

¹The code is available at: <https://github.com/SMRhadou/RobustUnrolling>.

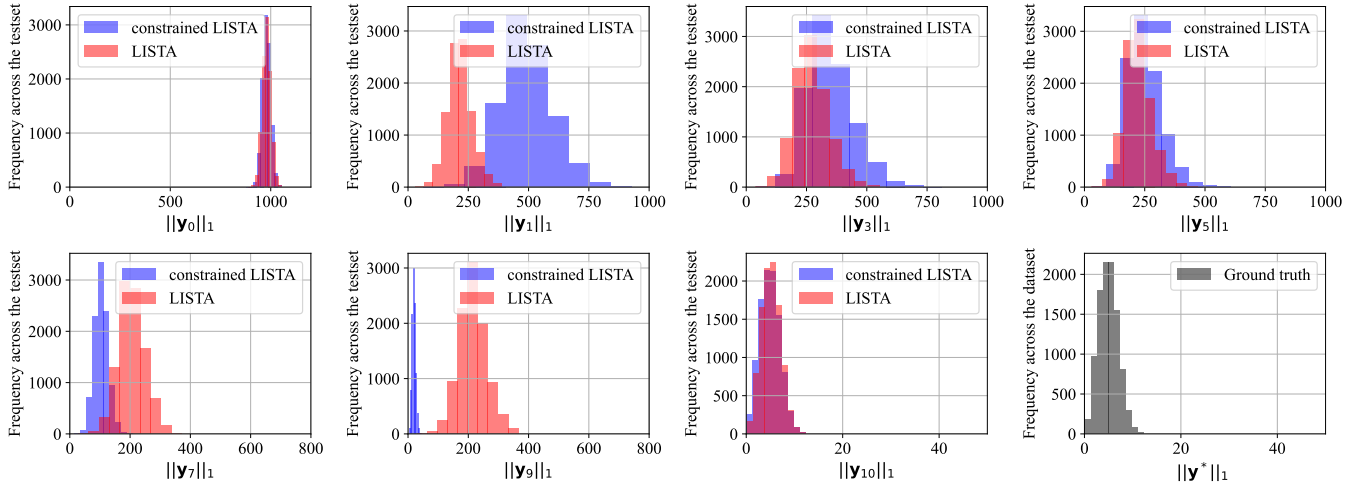


Fig. 4: Histogram of the ℓ_1 -norm of the unrolled layers’ outputs at (from top left to bottom right) the input, 1^{st} , 3^{th} , 5^{th} , 7^{th} , 9^{th} and 10^{th} layers along with the ground truth \mathbf{y}^* . The histogram stays the same across all the intermediate layers in the case of LISTA, while it moves to the left—representing lower values of ℓ_1 -norm—under the descending constraints.

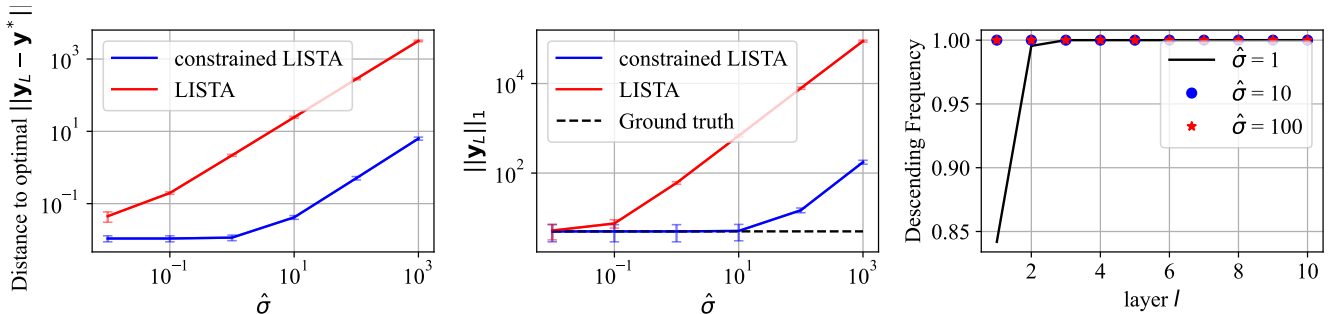


Fig. 5: Robustness against additive noise with a standard deviation proportional to the gradient by a factor $\hat{\sigma}$. (Left) Distance to the optimal \mathbf{y}^* , (middle) ℓ_1 -norm of the unrolled network’s output, and (right) Frequency of satisfying the constraints across the test dataset for different perturbation sizes.

witness in Figure 4 that the histogram of constrained LISTA is moving to the left over all the layers, implying a reduction in the ℓ_1 -norm at each and every layer.

Robustness. To examine the impact of the descending constraints, we show in Figure 5 the performance of LISTA and constrained LISTA after introducing additive perturbations at each unrolled layer. The perturbation is modeled by a noise vector, where each element is normally distributed with zero mean and a standard deviation of $\sigma_l = \hat{\sigma}g_l$. The figure confirms the robustness of constrained LISTA since the deterioration in both the distance to the optimal and the ℓ_1 -norm of the estimate is very slow compared to LISTA. Figure 5 (right) also shows that all the constraints were upheld in the case of constrained LISTA for different values of $\hat{\sigma}$, which confirms the robustness of the model.

V. CASE STUDY II: GENERATIVE FLOW MODELS FOR INPAINTING PROBLEMS

For our second case study, we present the inpainting problem, which is one of the challenging inverse problems. Following the same structure of the previous section, we first define the

inpainting problem, followed by a description of one method to unroll its solution with a generative model. We then discuss our constrained version of this solution and its robustness with the help of numerical simulations.

A. Problem Formulation

The inpainting problem is to predict image \mathbf{y} from a measurement $\mathbf{x} = \mathbf{A}\mathbf{y}$, where \mathbf{A} is a matrix masking the center elements of image \mathbf{y} . One common approach to solve this problem is through maximum a posteriori (MAP) inference, i.e., solving the optimization problem $\arg \max_{\mathbf{y}} p(\mathbf{x}|\mathbf{y})p_{\mu}(\mathbf{y})$. The likelihood $p(\mathbf{x}|\mathbf{y})$ in our case is a degenerate distribution that we approximate using a narrow Gaussian distribution $\mathcal{N}(\mathbf{A}\mathbf{y}, \sigma_n^2\mathbf{I})$. Under this distribution, the problem reduces to the (negative log posterior) problem

$$\arg \min_{\mathbf{y}} \frac{1}{2\sigma_n^2} \|\mathbf{x} - \mathbf{A}\mathbf{y}\|_2^2 - \log p_{\mu}(\mathbf{y}). \quad (16)$$

It is often the case that the prior distribution $p_{\mu}(\mathbf{y})$ is carefully chosen based on domain knowledge or modeled using a learnable generative model.

In our case study, we model the prior using the generative flow (GLOW) models [47]. GLOW transforms between a standard normal distribution $p(\mathbf{z}) \sim \mathcal{N}(0, \mathbf{I})$ of a latent variable \mathbf{z} and a more complex distribution using a series of *composable, bijective, and differentiable* mappings (or layers). These functions map each image to its latent representation, i.e.,

$$\mathbf{z} = h_\mu(\mathbf{y}) = (h_1 \circ \dots \circ h_i)(\mathbf{y}). \quad (17)$$

where \circ denotes a composition of functions and μ are learnable parameters. The inverse mappings, on the other hand, generate an image from a point in the latent space, i.e.,

$$\mathbf{y} = g_\mu(\mathbf{z}) = (h_i^{-1} \circ \dots \circ h_1^{-1})(\mathbf{z}). \quad (18)$$

Each mapping/layer h_* consists of actnorm, followed by an invertible 1×1 convolution, followed by a coupling layer. We refer the reader to Table 1 in [47] for a precise description of these operations.

Having these mappings learned leads to an exact evaluation of the prior distribution $p_\mu(\mathbf{y})$ in terms of the latent distribution [7], [48], [49]. Under the assumption that the latter is a standard normal distribution, the MAP problem in (16) can be transferred to the latent space leading to the problem

$$\arg \min_{\mathbf{z}} \|\mathbf{x} - \mathbf{A}g_\mu(\mathbf{z})\|_2^2 + \lambda \|\mathbf{z}\|_2^2, \quad (19)$$

where λ is a regularization parameter balancing the data consistency and the prior. Finding the optimal of (19) requires the generative model g_μ to be known apriori. This implies that learning the parameters of g_μ is executed separately before (19) is solved.

In this case study, we adopt the work in [7], which takes an alternative path in solving (19) through unrolling an iterative proximal-like algorithm.

B. Unrolled GLOW-Prox

A solution for (19) can be reached using a proximal-like algorithm that alternates between taking a gradient step in the direction of data consistency and projecting the solution to the proximity of the prior. The work in [7], which we refer to as unrolled GLOW-Prox, sets the parameters of this algorithm free to learn. More specifically, the l -th unrolled layer first updates the estimate using a gradient step,

$$\tilde{\mathbf{y}}_l = \mathbf{y}_{l-1} - \xi_l \mathbf{A}^\top (\mathbf{x} - \mathbf{A}\mathbf{y}_{l-1}), \quad (20)$$

where ξ_l is a learnable step size and the initial estimate \mathbf{y}_0 is set to be the masked image \mathbf{x} . This estimate is then converted to the latent space using a learnable GLOW network,

$$\tilde{\mathbf{z}}_l = h_\mu^{(l)}(\tilde{\mathbf{y}}_l). \quad (21)$$

This conversion is carried out so that a proximal update of the latent variable is executed next,

$$\mathbf{z}_l = \frac{\tilde{\mathbf{z}}_l}{1 + \zeta_l}, \quad (22)$$

where ζ_l is a learnable shrinkage parameter. The proximal update ensures that the estimate has a high likelihood by getting

\mathbf{z}_l closer to the origin, i.e., reducing its ℓ_2 -norm. Finally, we convert back to the signal space using the inverse map $g_\mu^{(l)}$,

$$\mathbf{y}_l = g_\mu^{(l)}(\mathbf{z}_l). \quad (23)$$

Hence, the estimate \mathbf{y}_l is a modified version of $\tilde{\mathbf{y}}_l$ that enhances the likelihood of the latent space. The learnable parameters at each layer are the scalars ξ_l and ζ_l and a full GLOW network $h_\mu^{(l)}$. Equations (20)-(23) are then repeated for L layers and the whole unrolled network is trained end-to-end to generate a final estimate $\mathbf{y}_L = \Phi(\mathbf{x}; \mathbf{W})$.

C. Constrained GLOW-Prox

Unlike [7], we perform a constrained-learning training procedure according to (CO). The unrolled network is trained by minimizing the mean square error between the output of unrolled GLOW-Prox and the true image,

$$\min_{\mathbf{W}} \mathbb{E}[\|\Phi(\mathbf{x}; \mathbf{W}) - \mathbf{y}\|_2^2]. \quad \text{s.t. (CI)}. \quad (24)$$

Here, we use two sets of the gradient constraints (CI) as we separate the variables \mathbf{y} and \mathbf{z} when computing the gradients, following the separation of their update rules in (20) and (22). In the first set of constraints, we force the gradient of the data consistency term with respect to \mathbf{y} , or $g_\mu(\mathbf{z})$, to descend, thereby ensuring that the update rule of \mathbf{z} in (22) does not drift the estimate \mathbf{y}_l away from $\tilde{\mathbf{y}}_l$. In other words, $\tilde{\mathbf{y}}_l$ is, by definition, chosen in the direction of the gradient while \mathbf{y}_l is forced to be in a descending direction using the imposed constraints. In the second set, we consider the gradients of the regularization term with respect to the latent variable \mathbf{z} to ensure that its likelihood is increasing over the layers. The training procedure follows Algorithm 1 except that two sets of dual variables are considered to accompany the two sets of constraints.

D. Numerical Results and Discussions

We assess the proposed constrained-learning approach on the CelebA-HQ dataset [50]. Each entry in the dataset is an RGB image with 64×64 pixels per color channel. To construct the corrupted images, we mask the center 24×24 pixels, and the goal is to inpaint the masked pixels to match the clean images. To achieve this, the unrolled GLOW-Prox is trained using pairs of corrupted and clean images $\{(\mathbf{x}_i, \mathbf{y}_i)\}_i$. The dataset consists of 17536 training, 976 validation and 976 test examples.

The unrolled GLOW-Prox consists of $L = 5$ layers. Each layer contains a GLOW network that has a depth of flow of 18 and 4 multi-scale levels [47]. We refer the reader to [7, Fig. 1] for a visualization of the network. We train the unrolled model to minimize (24) using ADAM with a learning rate $\mu_w = 10^{-5}$ and a dual learning rate $\mu_\lambda = 10^{-4}$. The constraint parameter ϵ is set to 0.05. As per (CO), we add a noise vector $\mathbf{n}_l \sim \mathcal{N}(0, \sigma_l^2 \mathbf{I})$ to the output of each unrolled layer l to ensure that the constraints are statistically independent. The noise variance declines over the layers, that is, $\sigma_l^2 \propto \frac{1}{l}$. The training is executed with mini-batches of size 8 and was held

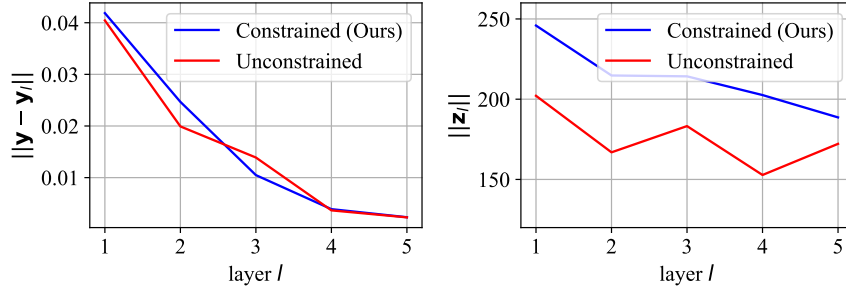


Fig. 6: Comparison between constrained and unconstrained GLOW-Prox. (Left) Distance to the original image y , averaged over the test dataset. (Right) The ℓ_2 -norm of the latent variable z_l , representing the negative log-likelihood.

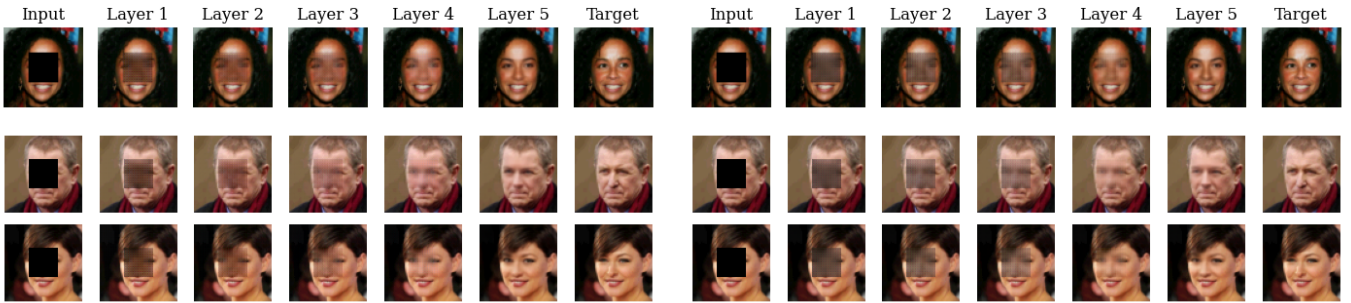


Fig. 7: Test examples of inpainted images across the unrolled layers of (left) constrained and (right) unconstrained GLOW-Prox. The performance of the two appears to be almost identical.

for 30 epochs.² We compare the performance and robustness of our constrained GLOW-Prox to the standard version trained without constraints [7].

Performance. We evaluate the distance, averaged over the test dataset, between the output of each unrolled layer and the clean images. The results are reported in Figure 6 (left), which shows that both constrained and unconstrained GLOW-Prox have a similar behavior in the image domain. This is also confirmed in Figure 7, which displays three test examples. As shown in the figure, the networks gradually inpaint the masked area reflecting a descending nature in the layers’ estimates. The two methods, however, depart from each other in the latent space, as shown in Figure 6 (right). The ℓ_2 -norm of the latent variable decreases gradually when the network is trained using constraints, implying that the gradient constraints were satisfied (and generalized) in the test examples. This is not the case when we omit the constraints during training, as depicted by the red line that fluctuates over the layers. However, we observe a gap in the ℓ_2 -norm between the two models, with the constrained one achieving higher norms across all the layers. This can be attributed to the noise added to the layers in the constrained case, which adds uncertainty to the network and reduces the log-likelihood.

Robustness. Despite the aforementioned slight drawback, constrained GLOW-Prox shows more robustness to input perturbations, as illustrated in Figure 8. The left plot in the figure shows the MSE between the original and reconstructed images after adding perturbations to the input image. The

perturbation is a random matrix $\frac{p\mathbf{N}}{\|\mathbf{N}\|_2}$, where \mathbf{N} is sampled from a standard normal distribution and p represents the perturbation size. As can be inferred from Figure 8 (left), the performance of the two models deteriorates with the perturbation size; however, GLOW-Prox deteriorates faster and more significantly than the constrained model. The distinction between the two models is more perceptible in Figure 8 (right), where the distortion in the shape of the facial features is more pronounced in the case of standard GLOW-Prox. In the case of constrained GLOW-Prox, the reconstructed images, albeit slightly different from the original, are still reasonably acceptable even under severe perturbations sizes.

VI. CONCLUSIONS

In this paper, we introduced a framework for posing unrolled networks as stochastic descent algorithms. Within this framework, the unrolled layers are trained with descending constraints to ensure that their trajectory of estimates descends toward a stationary point of the optimizee problem. Our theoretical analysis shows that this trajectory is guaranteed to converge with an exponential rate of convergence. These substantiated convergence guarantees confer two pivotal advantages upon unrolled networks, as demonstrated through our simulations. Firstly, the unrolled networks are guaranteed to generalize to previously unseen in-distribution problems. Secondly, they exhibit robustness to additive perturbations, thereby enhancing their out-of-distribution generalizability. These findings collectively underscore the potential of the proposed framework to contribute to the development of robust, interpretable unrolled networks for a wider array of applications.

²The code is available at: <https://github.com/SMRhadou/UnrolledGlow>.

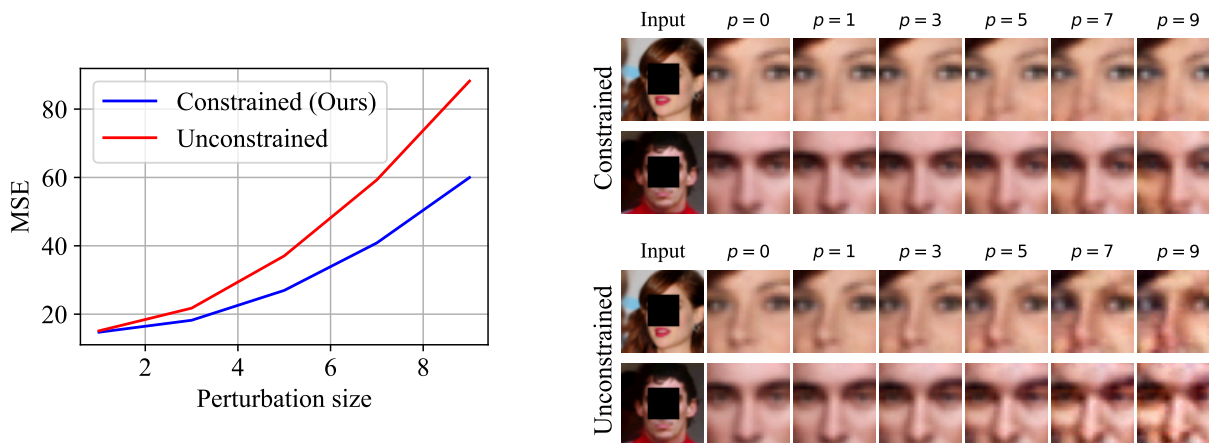


Fig. 8: Robustness. (Left) Mean square error between the original and reconstructed (inpainted) images under different perturbation sizes p . (Right) Examples of inpainted images using (top) constrained GLOW-Prox and (bottom) unconstrained GLOW-Prox for different p . Deterioration in the quality of the reconstructed images occurs faster in the unconstrained case.

APPENDIX A PROOF OF THEOREM 2

We describe the notation we use in our analysis followed by the proof of Theorem 2. Consider a probability space (Ω, \mathcal{F}, P) , where Ω is a sample space, \mathcal{F} is a sigma algebra, and $P : \mathcal{F} \rightarrow [0, 1]$ is a probability measure. We define a random variable $X : \Omega \rightarrow \mathbb{R}$ and write $P(\{\omega : X(\omega) = 0\})$ as $P(X = 0)$ to keep equations concise. We also define a filtration of \mathcal{F} as $\{\mathcal{F}_l\}_{l>0}$, which can be thought of as an increasing sequence of σ -algebras with $\mathcal{F}_{l-1} \subset \mathcal{F}_l$. We assume that the outputs of the unrolled layers \mathbf{y}_l are adapted to \mathcal{F}_l , i.e., $\mathbf{y}_l \in \mathcal{F}_l$.

Moreover, a stochastic process X_k is said to form a supermartingale if $\mathbb{E}[X_k | X_{k-1}, \dots, X_0] \leq X_{k-1}$. This inequality implies that given the past history of the process, the future value X_k is not, on average, larger than the latest one. In the following, we provide a proof to Theorem 2, which uses a supermartingale argument that is commonly used to prove convergence of stochastic descent algorithms.

Proof. Let $A_l \in \mathcal{F}_l$ be the event that the constraint (8) at layer l is satisfied. By the total expectation theorem, we have

$$\begin{aligned} \mathbb{E}[\|\nabla f(\mathbf{y}_l)\|] \\ = P(A_l)\mathbb{E}[\|\nabla f(\mathbf{y}_l)\| | A_l] + P(A_l^c)\mathbb{E}[\|\nabla f(\mathbf{y}_l)\| | A_l^c] \end{aligned} \quad (25)$$

with $P(A_l) = 1 - \delta$. Note that we write $f(\mathbf{y}_l; \mathbf{x})$ as $f(\mathbf{y}_l)$ for conciseness. The first term on the right-hand side is the conditional expectation conditioned on the constraint being met and, in turn, is bounded above according to (8). The second term represents the complementary event $A_l^c \in \mathcal{F}_l$. The conditional expectation in this case can also be bounded since the (conditional) expectation of a random variable cannot exceed its maximum value, i.e., $\mathbb{E}\|\nabla f(\mathbf{y}_l)\| \leq \max_{\mathbf{y}_l} \|\nabla f(\mathbf{y}_l)\|$, and the latter is bounded by M according to Assumption 1. Consequently, (25) is upper bounded by

$$\begin{aligned} \mathbb{E}[\|\nabla f(\mathbf{y}_l)\|] \\ \leq (1 - \delta)(1 - \epsilon) \mathbb{E}\|\nabla f(\mathbf{y}_{l-1})\| + (1 - \delta)\zeta(N, \delta) + \delta M, \end{aligned} \quad (26)$$

almost surely.

We then define a sequence of random variables with a degenerate distribution such that $Z_l = \mathbb{E}\|\nabla f(\mathbf{y}_l)\|$ almost surely for all l . We then construct a supermartingale-like inequality from (26):

$$\begin{aligned} \mathbb{E}[Z_l | \mathcal{F}_{l-1}] &\leq (1 - \delta)(1 - \epsilon) Z_{l-1} + (1 - \delta)\zeta(N, \delta) + \delta M \\ &= (1 - \delta) Z_{l-1} - (1 - \delta) \left(\epsilon Z_{l-1} - \zeta(N, \delta) - \frac{\delta M}{1 - \delta} \right). \end{aligned} \quad (27)$$

The goal of the rest of the proof is to show that i) when l grows, Z_l almost surely and infinitely often achieves values below $\eta := \frac{1}{\epsilon}(\zeta(N, \delta) + \delta M / (1 - \delta))$, and that ii) this also holds for the gradient norm $\|\nabla f(\mathbf{y}_l)\|$ itself.

To achieve the first objective, it suffices to show that the lowest gradient norm achieved, on average, up to layer l converges to a region of size η , i.e.,

$$\lim_{l \rightarrow \infty} \min_{k \leq l} \{Z_k\} \leq \eta \quad a.s. \quad (28)$$

To prove the above inequality, we define the sequences

$$\begin{aligned} \alpha_l &:= Z_l \cdot \mathbf{1}\{Z_l^{\text{best}} > \eta\}, \\ \beta_l &:= \left(\epsilon Z_l - \zeta(N, \delta) - \frac{\delta M}{1 - \delta} \right) \mathbf{1}\{Z_l^{\text{best}} > \eta\}, \end{aligned} \quad (29)$$

where $Z_l^{\text{best}} = \min_{k \leq l} \{Z_k\}$ and $\mathbf{1}\{\cdot\}$ is an indicator function. The first sequence α_l keeps the values of Z_l up until the best value Z_l^{best} drops below η for the first time. After this point, the best value stays below the threshold η since $Z_{l+1}^{\text{best}} \leq Z_l^{\text{best}}$ by definition. This ensures that the indication function stays at zero (i.e., $\alpha_l = 0$) for the rest of the sequence. Similarly, the sequence β_l follows the values of $\epsilon Z_l - \zeta(N, \delta) - \frac{\delta M}{1 - \delta}$ until it falls below zero for the first time.

We now aim to show that α_l forms a supermartingale, which requires finding an upper bound of the conditional expectation $\mathbb{E}[\alpha_l | \mathcal{F}_{l-1}]$. We use the total expectation theorem to write

$$\begin{aligned} \mathbb{E}[\alpha_l | \mathcal{F}_{l-1}] &= \mathbb{E}[\alpha_l | \mathcal{F}_{l-1}, \alpha_{l-1} = 0] P(\alpha_{l-1} = 0) \\ &\quad + \mathbb{E}[\alpha_l | \mathcal{F}_{l-1}, \alpha_{l-1} \neq 0] P(\alpha_{l-1} \neq 0), \end{aligned} \quad (30)$$

splitting the expectation into two cases: $\alpha_{l-1} = 0$ and $\alpha_{l-1} \neq 0$. When $\alpha_{l-1} = 0$, (29) implies that either Z_l or the indicator function is zero (i.e., $Z_l^{\text{best}} \leq \eta$). However, Z_l cannot be zero without $Z_l^{\text{best}} \leq \eta$, and, therefore, $\alpha_{l-1} = 0$ always implies that the indicator function is zero and $Z_l^{\text{best}} \leq \eta$. It also follows that β_{l-1} is zero when $\alpha_{l-1} = 0$ since it employs the same indicator function. As we discussed earlier, once $\alpha_{l-1} = 0$, all the values that follow is also zero, i.e., $\alpha_k = 0, \forall k \geq l-1$. Hence, the conditional expectation of α_l can be written as

$$\mathbb{E}[\alpha_l | \mathcal{F}_{l-1}, \alpha_{l-1} = 0] = (1 - \delta)(\alpha_{l-1} - \beta_{l-1}) = 0. \quad (31)$$

On the other hand, when $\alpha_{l-1} \neq 0$, the conditional expectation follows from the definition in (29),

$$\begin{aligned} \mathbb{E}[\alpha_l | \mathcal{F}_{l-1}, \alpha_{l-1} \neq 0] &= \mathbb{E}[Z_l \cdot \mathbf{1}\{Z_l^{\text{best}} > \eta\} | \mathcal{F}_{l-1}, \alpha_{l-1} \neq 0] \\ &\leq \mathbb{E}[Z_l | \mathcal{F}_{l-1}, \alpha_{l-1} \neq 0] \\ &\leq (1 - \delta) Z_{l-1} - (1 - \delta) \left(\epsilon Z_{l-1} - \zeta(N, \delta) - \frac{\delta M}{1 - \delta} \right) \\ &= (1 - \delta)(\alpha_{l-1} - \beta_{l-1}). \end{aligned} \quad (32)$$

The first inequality is true since the indicator function is at most one and the second inequality is a direct application of (27). The last equality results from that fact that the indicator function $\mathbf{1}\{Z_l^{\text{best}} > \eta\}$ is one since $\alpha_{l-1} \neq 0$, which implies that $\alpha_{l-1} = Z_{l-1}$ and $\beta_{l-1} = \epsilon Z_{l-1} - \zeta(N, \delta) - \frac{\delta}{1-\delta}M$.

Combining the results in (31) and (32) and substituting in (30), it finally follows that

$$\begin{aligned} \mathbb{E}[\alpha_l | \mathcal{F}_{l-1}] &\leq (1 - \delta)(\alpha_{l-1} - \beta_{l-1})[P(\alpha_{l-1} = 0) + P(\alpha_{l-1} \neq 0)] \\ &= (1 - \delta)(\alpha_{l-1} - \beta_{l-1}). \end{aligned} \quad (33)$$

It is worth noting that, for all l , $\alpha_l \geq 0$ and $\beta_l \geq 0$ by construction. It then follows from supermartingale convergence theorem [51, Theorem 1] that (33) implies that (i) α_l converges almost surely, and (ii) $\sum_{l=1}^{\infty} \beta_l$ is almost surely summable (i.e., finite). When the latter is written explicitly, we get

$$\sum_{l=1}^{\infty} \left(\epsilon Z_l - \zeta(N, \delta) - \frac{\delta M}{1 - \delta} \right) \mathbf{1}\{Z_l^{\text{best}} > \eta\} < \infty, \quad a.s., \quad (34)$$

The almost sure convergence of the above sequence implies that the limit inferior and limit superior coincide and

$$\liminf_{l \rightarrow \infty} \left(\epsilon Z_l - \zeta(N, \delta) - \frac{\delta M}{1 - \delta} \right) \mathbf{1}\{Z_l^{\text{best}} > \eta\} = 0, \quad a.s. \quad (35)$$

Equation (35) is true if either there exist a sufficiently large l such that $Z_l^{\text{best}} \leq \eta = \frac{1}{\epsilon}(\zeta(N, \delta) + \delta M / (1 - \delta))$ to set the indicator to zero or it holds that

$$\liminf_{l \rightarrow \infty} \left(\epsilon Z_l - \zeta(N, \delta) - \frac{\delta M}{1 - \delta} \right) = 0, \quad a.s. \quad (36)$$

which is equivalent to having $\sup_l \inf_{m \geq l} Z_m = \frac{1}{\epsilon}(\zeta(N, \delta) + \frac{\delta M}{1 - \delta})$. Hence, there exists some large l where $Z_l^{\text{best}} \leq \sup_l \inf_{m \geq l} Z_m$, which leads to the same upper bound. This proves the correctness of (28).

To this end, we have shown the convergence of Z_l^{best} , which was defined as the best *expected* value of $\|\nabla f(\mathbf{y}_l)\|$. Now, we turn to show the convergence of the random variable $\|\nabla f(\mathbf{y}_l)\|$ itself. We use that the fact that $Z_l = \int \|\nabla f(\mathbf{y}_l)\| dP$ to re-write (36) as

$$\liminf_{l \rightarrow \infty} \int \epsilon \|\nabla f(\mathbf{y}_l)\| dP = \zeta(N, \delta) + \frac{\delta M}{1 - \delta}, \quad a.s. \quad (37)$$

By Fatou's lemma [52, Theorem 1.5.5], it follows that

$$\begin{aligned} \int \liminf_{l \rightarrow \infty} \epsilon \|\nabla f(\mathbf{y}_l)\| dP &\leq \liminf_{l \rightarrow \infty} \int \epsilon \|\nabla f(\mathbf{y}_l)\| dP \\ &= \zeta(N, \delta) + \frac{\delta M}{1 - \delta}. \end{aligned} \quad (38)$$

We can bound the left-hand side from below by defining $f_l^{\text{best}} := \min_{k \leq l} \|\nabla f(\mathbf{y}_k)\|$ as the lowest gradient norm achieved up to layer l . By definition, $f_l^{\text{best}} \leq \liminf_{l \rightarrow \infty} \|\nabla f(\mathbf{y}_l)\|$ for sufficiently large l . Therefore, we get

$$\begin{aligned} \epsilon \int f_l^{\text{best}} dP &\leq \epsilon \int \liminf_{l \rightarrow \infty} \|\nabla f(\mathbf{y}_l)\| dP \\ &\leq \zeta(N, \delta) + \frac{\delta M}{1 - \delta}, \quad a.s. \end{aligned} \quad (39)$$

for some large l . Equivalently, we can write that

$$\lim_{l \rightarrow \infty} \int f_l^{\text{best}} dP \leq \frac{1}{\epsilon} \left(\zeta(N, \delta) + \frac{\delta M}{1 - \delta} \right), \quad a.s. \quad (40)$$

which completes the proof. \square

APPENDIX B PROOF OF LEMMA 1

Similar to the proof in Appendix A, we write $f(\mathbf{y}_l; \mathbf{x})$ as $f(\mathbf{y}_l)$ for conciseness.

Proof. First, we recursively unroll the right-hand side of (26) to evaluate the reduction in the gradient norm $\mathbb{E}\|\nabla f(\mathbf{y}_l)\|$ after l layers. The gradient norm at the l -th layer then satisfies

$$\begin{aligned} \mathbb{E}[\|\nabla f(\mathbf{y}_l)\|] &\leq (1 - \delta)^l (1 - \epsilon)^l \mathbb{E}\|\nabla f(\mathbf{y}_0)\| \\ &\quad + \sum_{i=0}^{l-1} (1 - \delta)^{i-1} (1 - \epsilon)^{i-1} \left[(1 - \delta)\zeta(N, \delta) + \delta M \right]. \end{aligned} \quad (41)$$

The summation on the right-hand side resembles a geometric sum, which can be simplified to

$$\begin{aligned} \mathbb{E}[\|\nabla f(\mathbf{y}_l)\|] &\leq (1 - \delta)^l (1 - \epsilon)^l \mathbb{E}\|\nabla f(\mathbf{y}_0)\| \\ &\quad + \frac{1 - (1 - \delta)^l (1 - \epsilon)^l}{1 - (1 - \delta)(1 - \epsilon)} \left[(1 - \delta)\zeta(N, \delta) + \delta M \right]. \end{aligned} \quad (42)$$

Second, we aim to evaluate the distance between the gradient norm at the L -th layer and its optimal value,

$$\begin{aligned} &\left| \mathbb{E}[\|\nabla f(\mathbf{y}_L)\|] - \mathbb{E}[\|\nabla f(\mathbf{y}^*)\|] \right| \\ &= \lim_{l \rightarrow \infty} \left| \mathbb{E}[\|\nabla f(\mathbf{y}_L)\|] - \mathbb{E}[\min_{k \leq l} \|\nabla f(\mathbf{y}_k)\|] \right| \\ &\quad + \left| \mathbb{E}[\min_{k \leq l} \|\nabla f(\mathbf{y}_k)\|] - \mathbb{E}[\|\nabla f(\mathbf{y}^*)\|] \right|. \end{aligned} \quad (43)$$

In (43), we add and subtract $\lim_{l \rightarrow \infty} \mathbb{E}[\min_{k \leq l} \|\nabla f(\mathbf{y}_k)\|]$ in the right-hand side while imposing the limit when l goes to infinity. Using triangle inequality, we re-write (43) as

$$\begin{aligned} & \left| \mathbb{E}[\|\nabla f(\mathbf{y}_L)\|] - \mathbb{E}[\|\nabla f(\mathbf{y}^*)\|] \right| \\ & \leq \lim_{l \rightarrow \infty} \left| \mathbb{E}[\|\nabla f(\mathbf{y}_L)\|] - \mathbb{E}[\min_{k \leq l} \|\nabla f(\mathbf{y}_k)\|] \right| \\ & \quad + \lim_{l \rightarrow \infty} \left| \mathbb{E}[\min_{k \leq l} \|\nabla f(\mathbf{y}_k)\|] - \mathbb{E}[\|\nabla f(\mathbf{y}^*)\|] \right|. \end{aligned} \quad (44)$$

Note that the gradient of f at the stationary point \mathbf{y}^* is zero. Therefore, the second term on the right-hand side is upper bounded according to Theorem 2.

The final step required to prove Lemma 1 is to evaluate the first term in (44). To do so, we observe that

$$\begin{aligned} & \lim_{l \rightarrow \infty} \left| \mathbb{E}[\|\nabla f(\mathbf{y}_L)\|] - \mathbb{E}[\min_{k \leq l} \|\nabla f(\mathbf{y}_k)\|] \right| = \\ & \quad \mathbb{E}[\|\nabla f(\mathbf{y}_L)\|] - \lim_{l \rightarrow \infty} \mathbb{E}[\min_{k \leq l} \|\nabla f(\mathbf{y}_k)\|]. \end{aligned} \quad (45)$$

This is the case since $\mathbb{E}[\|\nabla f(\mathbf{y}_l)\|]$ cannot go below the minimum of the gradient norm when l goes to infinity. Next, we substitute (42) in (45)

$$\begin{aligned} & \left| \mathbb{E}[\|\nabla f(\mathbf{y}_L)\|] - \lim_{l \rightarrow \infty} \mathbb{E}[\min_{k \leq l} \|\nabla f(\mathbf{y}_k)\|] \right| \\ & = (1 - \delta)^L (1 - \epsilon)^L \mathbb{E}[\|\nabla f(\mathbf{y}_0)\|] \\ & \quad + \frac{1 - (1 - \delta)^L (1 - \epsilon)^L}{1 - (1 - \delta)(1 - \epsilon)} \left[(1 - \delta)\zeta(N, \delta) + \delta M \right] \\ & \quad - \lim_{l \rightarrow \infty} (1 - \delta)^l (1 - \epsilon)^l \mathbb{E}[\|\nabla f(\mathbf{y}_0)\|] \\ & \quad - \lim_{l \rightarrow \infty} \frac{1 - (1 - \delta)^l (1 - \epsilon)^l}{1 - (1 - \delta)(1 - \epsilon)} \left[(1 - \delta)\zeta(N, \delta) + \delta M \right]. \end{aligned} \quad (46)$$

The first limit in (46) goes to zero since $(1 - \delta)(1 - \epsilon) < 1$, and the second limit is evaluated as the constant $\frac{(1 - \delta)\zeta(N, \delta) + \delta M}{1 - (1 - \delta)(1 - \epsilon)}$. Therefore, we get

$$\begin{aligned} & \left| \mathbb{E}[\|\nabla f(\mathbf{y}_L)\|] - \lim_{l \rightarrow \infty} \mathbb{E}[\min_{k \leq l} \|\nabla f(\mathbf{y}_k)\|] \right| \\ & = (1 - \delta)^L (1 - \epsilon)^L \mathbb{E}[\|\nabla f(\mathbf{y}_0)\|] \\ & \quad - \frac{(1 - \delta)^L (1 - \epsilon)^L}{1 - (1 - \delta)(1 - \epsilon)} \left[(1 - \delta)\zeta(N, \delta) + \delta M \right] \\ & \leq (1 - \delta)^L (1 - \epsilon)^L \mathbb{E}[\|\nabla f(\mathbf{y}_0)\|]. \end{aligned} \quad (47)$$

The last inequality follows since the term $\frac{(1 - \delta)^L (1 - \epsilon)^L}{1 - (1 - \delta)(1 - \epsilon)} [(1 - \delta)\zeta(N, \delta) + \delta M]$ is nonnegative. Combining the two results, i.e., (44) and (47), we can get the upper bound

$$\begin{aligned} & \left| \mathbb{E}[\|\nabla f(\mathbf{y}_L)\|] - \mathbb{E}[\|\nabla f(\mathbf{y}^*)\|] \right| \\ & \leq (1 - \delta)^L (1 - \epsilon)^L \mathbb{E}[\|\nabla f(\mathbf{y}_0)\|] \\ & \quad + \frac{1}{\epsilon} \left(\zeta(N, \delta) + \frac{\delta M}{1 - \delta} \right), \end{aligned} \quad (48)$$

which completes the proof. \square

REFERENCES

- [1] K. Gregor and Y. LeCun, "Learning fast approximations of sparse coding," in *Proceedings of the 27th International Conference on International Conference on Machine Learning, ICM'10*, pp. 399–406, June 2010.
- [2] Y. Yang, D. P. Wipf, et al., "Transformers from an optimization perspective," *Advances in Neural Information Processing Systems*, vol. 35, pp. 36958–36971, 2022.
- [3] Y. Yu, S. Buchanan, D. Pai, T. Chu, Z. Wu, S. Tong, B. D. Haeffele, and Y. Ma, "White-box transformers via sparse rate reduction," *arXiv preprint arXiv:2306.01129*, 2023.
- [4] J. Von Oswald, E. Niklasson, E. Randazzo, J. Sacramento, A. Mordvintsev, A. Zhmoginov, and M. Vladymyrov, "Transformers learn in-context by gradient descent," in *International Conference on Machine Learning*, pp. 35151–35174, PMLR, 2023.
- [5] V. Monga, Y. Li, and Y. C. Eldar, "Algorithm unrolling: Interpretable, efficient deep learning for signal and image processing," *IEEE Signal Processing Magazine*, vol. 38, pp. 18–44, Mar. 2021.
- [6] K. Zhang, L. V. Gool, and R. Timofte, "Deep unfolding network for image super-resolution," in *Proceedings of the IEEE/CVF conference on computer vision and pattern recognition*, pp. 3217–3226, 2020.
- [7] X. Wei, H. van Gorp, L. Gonzalez-Carabarin, D. Freedman, Y. C. Eldar, and R. J. G. van Sloun, "Deep unfolding with normalizing flow priors for inverse problems," *IEEE Transactions on Signal Processing*, vol. 70, pp. 2962–2971, 2022.
- [8] C. Mou, Q. Wang, and J. Zhang, "Deep generalized unfolding networks for image restoration," in *Proceedings of the IEEE/CVF Conference on Computer Vision and Pattern Recognition*, pp. 17399–17410, 2022.
- [9] Y. Li, M. Tofighi, J. Geng, V. Monga, and Y. C. Eldar, "Efficient and interpretable deep blind image deblurring via algorithm unrolling," *IEEE Transactions on Computational Imaging*, vol. 6, pp. 666–681, 2020.
- [10] P. Qiao, S. Liu, T. Sun, K. Yang, and Y. Dou, "Towards vision transformer unrolling fixed-point algorithm: a case study on image restoration," *arXiv preprint arXiv:2301.12332*, 2023.
- [11] Q. Hu, Y. Cai, Q. Shi, K. Xu, G. Yu, and Z. Ding, "Iterative algorithm induced deep-unfolding neural networks: Precoding design for multiuser mimo systems," *IEEE Transactions on Wireless Communications*, vol. 20, no. 2, pp. 1394–1410, 2020.
- [12] A. Chowdhury, G. Verma, C. Rao, A. Swami, and S. Segarra, "Unfolding wmmse using graph neural networks for efficient power allocation," *IEEE Transactions on Wireless Communications*, vol. 20, no. 9, pp. 6004–6017, 2021.
- [13] Y. Liu, Q. Hu, Y. Cai, G. Yu, and G. Y. Li, "Deep-unfolding beamforming for intelligent reflecting surface assisted full-duplex systems," *IEEE Transactions on Wireless Communications*, vol. 21, no. 7, pp. 4784–4800, 2021.
- [14] L. Schynol and M. Pesavento, "Coordinated sum-rate maximization in multicell mu-mimo with deep unrolling," *IEEE Journal on Selected Areas in Communications*, vol. 41, no. 4, pp. 1120–1134, 2023.
- [15] H. Huang, Y. Lin, G. Gui, H. Gacanian, H. Sari, and F. Adachi, "Regularization strategy aided robust unsupervised learning for wireless resource allocation," *IEEE Transactions on Vehicular Technology*, 2023.
- [16] H. Yang, N. Cheng, R. Sun, W. Quan, R. Chai, K. Aldubaikhy, A. Alqasir, and X. Shen, "Knowledge-driven resource allocation for d2d networks: A wmmse unrolled graph neural network approach," *arXiv preprint arXiv:2307.05882*, 2023.
- [17] Y. Li, O. Bar-Shira, V. Monga, and Y. C. Eldar, "Deep algorithm unrolling for biomedical imaging," *arXiv preprint arXiv:2108.06637*, 2021.
- [18] U. Nakarmi, J. Y. Cheng, E. P. Rios, M. Mardani, J. M. Pauly, L. Ying, and S. S. Vasanaawala, "Multi-scale unrolled deep learning framework for accelerated magnetic resonance imaging," in *2020 IEEE 17th International Symposium on Biomedical Imaging (ISBI)*, pp. 1056–1059, IEEE, 2020.
- [19] N. Chennakeshava, T. S. Stevens, F. J. de Bruijn, A. Hancock, M. Pekař, Y. C. Eldar, M. Mischi, and R. J. van Sloun, "Deep proximal unfolding for image recovery from under-sampled channel data in intravascular ultrasound," in *ICASSP 2022-2022 IEEE International Conference on Acoustics, Speech and Signal Processing (ICASSP)*, pp. 1221–1225, IEEE, 2022.
- [20] H. Wang, Y. Li, H. Zhang, D. Meng, and Y. Zheng, "Indudonet+: A deep unfolding dual domain network for metal artifact reduction in ct images," *Medical Image Analysis*, vol. 85, p. 102729, 2023.
- [21] S. Hadou, N. NaderiAlizadeh, and A. Ribeiro, "Stochastic unrolled federated learning," *arXiv preprint arXiv:2305.15371*, 2023.
- [22] S. Ravi and H. Larochelle, "Optimization as a model for few-shot learning," in *International Conference on Learning Representations*, 2016.

- [23] J. R. Hershey, J. L. Roux, and F. Weninger, “Deep unfolding: Model-based inspiration of novel deep architectures,” *arXiv preprint arXiv:1409.2574*, 2014.
- [24] R. Nasser, Y. C. Eldar, and R. Sharan, “Deep unfolding for non-negative matrix factorization with application to mutational signature analysis,” *Journal of Computational Biology*, vol. 29, no. 1, pp. 45–55, 2022.
- [25] Y. Noah and N. Shlezinger, “Limited communications distributed optimization via deep unfolded distributed admm,” *arXiv preprint arXiv:2309.14353*, 2023.
- [26] C. Liu, G. Leus, and E. Isufi, “Unrolling of simplicial elasticnet for edge flow signal reconstruction,” *IEEE Open Journal of Signal Processing*, pp. 1–9, 2023.
- [27] H. Heaton, X. Chen, Z. Wang, and W. Yin, “Safeguarded learned convex optimization,” *Proceedings of the AAAI Conference on Artificial Intelligence*, vol. 37, pp. 7848–7855, Jun. 2023.
- [28] J. Shen, X. Chen, H. Heaton, T. Chen, J. Liu, W. Yin, and Z. Wang, “Learning a minimax optimizer: A pilot study,” in *International Conference on Learning Representations*, 2021.
- [29] M. Moeller, T. Mollenhoff, and D. Cremers, “Controlling neural networks via energy dissipation,” in *Proceedings of the IEEE/CVF International Conference on Computer Vision (ICCV)*, October 2019.
- [30] R. Liu, P. Mu, and J. Zhang, “Investigating customization strategies and convergence behaviors of task-specific admm,” *IEEE Transactions on Image Processing*, vol. 30, pp. 8278–8292, 2021.
- [31] X. Chen, J. Liu, Z. Wang, and W. Yin, “Theoretical linear convergence of unfolded ista and its practical weights and thresholds,” in *Advances in Neural Information Processing Systems*, vol. 31, 2018.
- [32] J. Liu, X. Chen, Z. Wang, and W. Yin, “ALISTA: Analytic weights are as good as learned weights in LISTA,” in *International Conference on Learning Representations*, 2019.
- [33] X. Xie, J. Wu, G. Liu, Z. Zhong, and Z. Lin, “Differentiable linearized ADMM,” in *Proceedings of the 36th International Conference on Machine Learning*, vol. 97 of *Proceedings of Machine Learning Research*, pp. 6902–6911, PMLR, 09–15 Jun 2019.
- [34] M. Abadi, A. Chu, I. Goodfellow, H. B. McMahan, I. Mironov, K. Talwar, and L. Zhang, “Deep learning with differential privacy,” in *Proceedings of the 2016 ACM SIGSAC Conference on Computer and Communications Security, CCS ’16*, p. 308–318, 2016.
- [35] S. Hadou, C. I. Kanatsoulis, and A. Ribeiro, “Space-time graph neural networks with stochastic graph perturbations,” in *IEEE International Conference on Acoustics, Speech and Signal Processing (ICASSP)*, pp. 1–5, 2023.
- [36] S. Hadou, C. I. Kanatsoulis, and A. Ribeiro, “Space-time graph neural networks,” in *International Conference on Learning Representations (ICLR)*, 2022.
- [37] F. Gama, J. Bruna, and A. Ribeiro, “Stability properties of graph neural networks,” *IEEE Transactions on Signal Processing*, vol. 68, pp. 5680–5695, 2020.
- [38] M. Andrychowicz, M. Denil, S. G. Colmenarejo, M. W. Hoffman, D. Pfau, T. Schaul, B. Shillingford, and N. de Freitas, “Learning to learn by gradient descent by gradient descent,” in *Proceedings of the 30th International Conference on Neural Information Processing Systems*, p. 3988–3996, 2016.
- [39] R. Liu, X. Liu, S. Zeng, J. Zhang, and Y. Zhang, “Optimization-derived learning with essential convergence analysis of training and hyper-training,” in *International Conference on Machine Learning*, pp. 13825–13856, PMLR, 2022.
- [40] L. F. Chamon, S. Paternain, M. Calvo-Fullana, and A. Ribeiro, “Constrained learning with non-convex losses,” *IEEE Transactions on Information Theory*, 2022.
- [41] S. P. Boyd and L. Vandenberghe, *Convex optimization*. Cambridge university press, 2004.
- [42] I. Daubechies, M. Defrise, and C. De Mol, “An iterative thresholding algorithm for linear inverse problems with a sparsity constraint,” *Communications on Pure and Applied Mathematics*, vol. 57, no. 11, pp. 1413–1457, 2004.
- [43] A. Beck and M. Teboulle, “A fast iterative shrinkage-thresholding algorithm with application to wavelet-based image deblurring,” in *2009 IEEE International Conference on Acoustics, Speech and Signal Processing*, pp. 693–696, Apr. 2009.
- [44] H. Chung, S. J. Lee, and J. G. Park, “Deep neural network using trainable activation functions,” in *2016 International Joint Conference on Neural Networks (IJCNN)*, pp. 348–352, 2016.
- [45] S. Kiliçarslan and M. Celik, “Rsigelu: A nonlinear activation function for deep neural networks,” *Expert Systems with Applications*, vol. 174, p. 114805, 2021.
- [46] M. Varshney and P. Singh, “Optimizing nonlinear activation function for convolutional neural networks,” *Signal, Image and Video Processing*, vol. 15, no. 6, pp. 1323–1330, 2021.
- [47] D. P. Kingma and P. Dhariwal, “Glow: Generative flow with invertible 1x1 convolutions,” *Advances in neural information processing systems*, vol. 31, 2018.
- [48] M. Asim, M. Daniels, O. Leong, A. Ahmed, and P. Hand, “Invertible generative models for inverse problems: mitigating representation error and dataset bias,” in *International Conference on Machine Learning*, pp. 399–409, PMLR, 2020.
- [49] J. Whang, Q. Lei, and A. Dimakis, “Solving inverse problems with a flow-based noise model,” in *International Conference on Machine Learning*, pp. 11146–11157, PMLR, 2021.
- [50] T. Karras, T. Aila, S. Laine, and J. Lehtinen, “Progressive growing of gans for improved quality, stability, and variation,” *arXiv preprint arXiv:1710.10196*, 2017.
- [51] H. Robbins and D. Siegmund, “A convergence theorem for non negative almost supermartingales and some applications,” in *Optimizing Methods in Statistics*, pp. 233–257, Academic Press, Jan. 1971.
- [52] R. Durrett, *Probability: theory and examples*, vol. 49. Cambridge university press, 2019.